SYNTHETIC BIOLOGY

# Spatial interference scale as a determinant of microbial range expansion

Venhar Celik Ozgen[1,2,3]*, Wentao Kong[1,3]*, Andrew E. Blanchard[3,4]*, Feng Liu[1,3], Ting Lu[1,3,4,5,6]†



**In microbial communities, social interactions such as competition occur ubiquitously across multiple spatial scales from local proximity to remote distance. However, it remains unclear how such a spatial variation of interaction contributes to the structural development of microbial populations. Here, we developed synthetic consortia, biophysical theory, and simulations to elucidate the role of spatial interference scale in governing ecosystem organization during range expansion. For consortia with unidirectional interference, we discovered that, at growing fronts, the extinction time of toxin-sensitive species is reciprocal to the spatial interference scale. In contrast, for communities with bidirectional interference, their structures diverge into distinct monoculture colonies under different initial conditions, with the corresponding separatrix set by the spatial scale of interference. Near the separatrix, ecosystem development becomes noise-driven and yields opposite structures. Our results establish spatial interaction scale as a key determinant for microbial range expansion, providing insights into microbial spatial organization and synthetic ecosystem engineering.**

## INTRODUCTION

Microbial communities often form heterogeneous structures in space. For instance, in laboratory settings, they can aggregate into concentric rings (*1*), spiral vortexes (*2*), and radial arrays of spots (*3*); in natural environments, microbes further develop into single- or multispecies biofilms that exhibit a remarkable degree of complexity (*4*, *5*). These structures arise from diverse biotic and abiotic processes, among which cellular social interactions such as competition serve as a major driving force (*6*–*10*). Ubiquitous in the microbial world, social interactions are recently found to be highly diverse in spatial scale (*11*). For example, they can occur in close proximity via mechanisms such as C signaling in *Myxococcus xanthus* (*12*), crisscross signaling in *Bacillus subtilis* (*13*), and contact-dependent inhibition in *Escherichia coli* (*14*). Alternatively, social interactions may take place over distance through the diffusion of ions such as potassium (*15*), small metabolites such as acyl-homoserine lactone (AHL) of *Vibrio fischeri* (*16*), and membrane vesicles of *Pseudomonas aeruginosa* (*17*).

As social interactions profoundly affect community organization, such a spatial variation of interactions invites a fundamental question: How does the spatial scale of interactions contribute to microbial ecosystem growth in space and time? Answering the question is important, as it will provide insights into the processes and patterns underlying microbial ecology and, hence, advance our knowledge about the organizational principles of native ecosystems (*9*, *18*, *19*). It will also aid in the development of synthetic microbial ecosystems with desired structures and robust functions for next-generation biotechnological applications (*20*).

Here, we tackled the question by choosing competition as our model social interaction because it is the most prevalent among all types of microbial interactions (*21*). We also used spatial range expansion as the model process for ecosystem development, as it is a commonly observed mode of microbial dynamics, with examples including bacterial colonization in new habitats and initial growth of biofilms on surfaces (*22*). In addition, range expansion has relatively simple spatiotemporal dynamics but has the essential characteristics common in natural communities (*23*, *24*). Furthermore, similar dynamics occurs in living organisms beyond microbes at distinct length and time scales, such as the migration of humans out of Africa (*25*), ongoing expansion of western bluebirds across the northwestern United States (*26*), and latest invasion of cane toads in Australia (*27*).

We developed engineered microbial communities—ecosystems with artificially created cellular interactions—as our experimental systems, owing to their reduced system complexity and enhanced amenability compared to native ecosystems, as demonstrated by recent examples (*28*–*36*). In parallel, we derived a biophysical theory and constructed individual-based simulations to quantitatively describe and further generalize our findings from the experiment. Our study showed that, for ecosystems with unidirectional interference, there is a space-to-time translation at growing fronts, i.e., the extinction time of toxin-sensitive species is reciprocal to the spatial interference scale. In contrast, for communities with bidirectional interference, their structures diverge into distinct monoculture colonies under different initial conditions, determined by the relative diffusion lengths of the two toxins. Together, our results provide important insights into the roles of the spatial interference scale in determining microbial ecosystem growth in space.

## RESULTS

### Synthetic microbial consortia confer two distinct scales of interference in space

We began our investigation by constructing a pair of two-strain *E. coli* consortia, including one with contact-dependent short-range inhibition (SRI) (Fig. 1A) and the other involving diffusion-based long-range inhibition (LRI) (Fig. 1B). The SRI consortium consists of a toxin-producing strain (SRI+), created by introducing a copy of the constitutively expressed contact-dependent inhibition operon (*cdiBAI*) into the *E. coli* strain EPI300 (*14*) and a sensitive strain (SRI–) established by loading the vector pCC1BAC into another copy of EPI300 (Fig. 1C

[1]Department of Bioengineering, University of Illinois at Urbana-Champaign, Urbana, IL 61801, USA. [2]Department of Bioengineering, Faculty of Engineering, University of Firat, 23119 Elazig, Turkey. [3]Carl R. Woese Institute for Genomic Biology, University of Illinois at Urbana-Champaign, Urbana, IL 61801, USA. [4]Department of Physics, University of Illinois at Urbana-Champaign, Urbana, IL 61801, USA. [5]Center for Biophysics and Quantitative Biology, University of Illinois at Urbana-Champaign, Urbana, IL 61801, USA. [6]National Center for Supercomputing Applications, University of Illinois at Urbana-Champaign, Urbana, IL 61801, USA.
*These authors contributed equally to this work.
†Corresponding author. Email: luting@illinois.edu

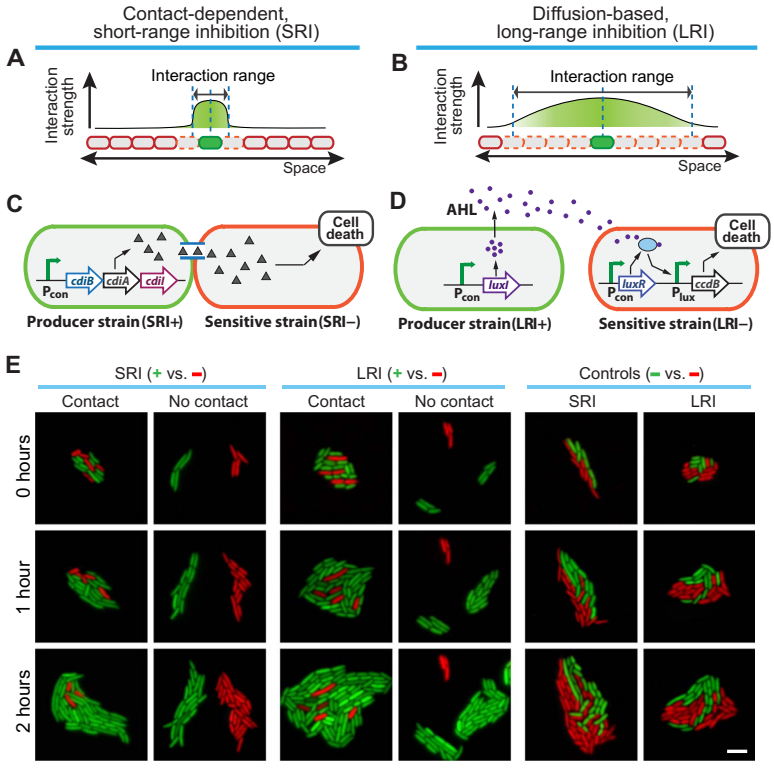


**Fig. 1. Synthetic microbial consortia that confer short- and long-range interference in space.** (**A**) Conceptual illustration of SRI that is harmful to nearest neighbors only. (**B**) Conceptual illustration of LRI that is detrimental to cells within a distance. (**C**) Circuit diagram of the synthetic SRI consortium composed of a toxin-producing strain (SRI+) and a sensitive strain (SRI–). In SRI+, a constitutive promoter drives the contact-dependent inhibition operon, *cdiBAI*, allowing SRI+ to suppress SRI– by injecting toxins via physical contact. (**D**) Circuit diagram of the synthetic LRI consortium consisting of a toxin-producing strain (LRI+) and a sensitive strain (LRI–). In LRI+, a constitutive promoter drives the *luxI* gene. In LRI–, a constitutive promoter drives *luxR* and the AHL-responsive promoter $P_{lux}$ drives *ccdB*. LuxI in LRI+ enzymatically produces a small-molecule AHL, which secretes into the extracellular milieu and further diffuses into other cells; induced by AHL, CcdB production in LRI– results in its growth inhibition. (**E**) Single-cell snapshots of the synthetic consortia growing on agar pads. Left columns: The SRI consortium (green, SRI+; red, SRI–); middle columns: The LRI consortium (green, LRI+; red, LRI–); and right columns: A consortium of two SRI– strains (left) and two LRI– strains (right). Scale bar, 4 μm.

and fig. S1, A and B). Here, SRI+ inhibits the growth of SRI– by injecting toxins (CdiA) into the latter through direct contact. The LRI consortium is composed of a toxin-producing strain (LRI+) and a sensitive strain (LRI–), which were developed by introducing the constitutively expressed *luxI* gene (*37*) into one copy of EPI300 and the constitutively expressed *luxR* gene (*37*) and the AHL-inducible toxin *ccdB* gene (*38*) into another copy of EPI300, respectively [Fig. 1D and figs. S1 (C and D) and S2 (A and B)]. In this design, LRI+ produces AHL that diffuses over distance to trigger the toxin synthesis and hence apoptosis of LRI–. For both consortia, *yemGFP* and *mKate2* were integrated into the chromosomes of the producer and sensitive strains, respectively, for visualization and quantitative analysis (table S1).

To validate the designed cellular interactions, we examined the single-cell dynamics of the consortia using time-lapse microscopy (Materials and Methods). For the SRI consortium, we found that SRI+ inhibited SRI– when they were in direct contact (Fig. 1E, column 1); however, when separated, SRI+ and SRI– both grew (Fig. 1E, column 2). In contrast, for the LRI consortium, LRI+ always inhibited the growth of LRI– regardless of the distance (Fig. 1E, columns 3 and 4). For comparison, all strains were able to grow even when in direct contact, as long as their interactions were abolished (Fig. 1E, columns 5 and 6). Using these consortia, we also performed coculture experiments and confirmed that both producers were able to effectively inhibit the growth of the sensitive strains (fig. S2, C and D).

## Ecosystem range expansion reveals a reciprocal relationship between spatial interference scale and extinction time

We next tested the spatial development of the consortia through solid agar range expansion experiments (Materials and Methods). Here, range expansion was chosen as the model process of community assembly because it involves relatively simple spatiotemporal dynamics while still preserving the essential characteristics common in natural communities (*23*). Our results showed that, in the absence of interference (Fig. 2, A and C), strains of each consortium remained roughly equal at the expanding fronts over the course of 96 hours. However, when inference was present (Fig. 2, B and D), the toxin producers always outperformed the sensitive and occupied the entire expanding fronts eventually. The results also showed that, during range expansion, the toxin producer (SRI+) of the SRI consortium became increasingly abundant over time and drove the sensitive to extinction at the front at around 48 hours (Fig. 2B), whereas in the LRI consortium, the toxin producer (LRI+) took over the space within 12 hours and fully dominated at the front throughout the experiment (Fig. 2D). To rule out the possibility that the observed structural differences were caused by the growth rate difference of the strains, we repeated the experiments using strains whose fluorescence reporters were swapped (Fig. 2E). Notably, growing from the initial mixtures, a subset of small close sectors first merged into big sectors before gradually disappearing (sensitive sectors) or expanding (toxin-producing sectors) later,

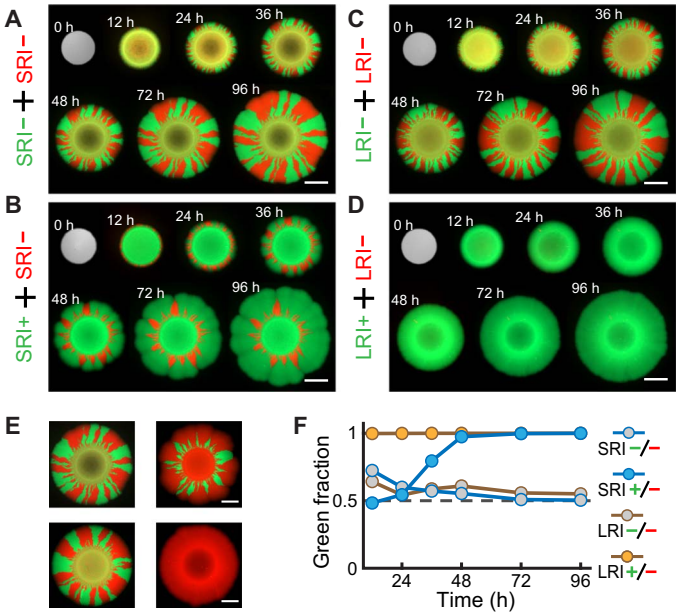


**Fig. 2. Range expansion dynamics of the microbial consortia with distinct scales of interference.** (**A** to **D**) Snapshots of typical range expansion dynamics of the four consortia, which are composed of two SRI– strains (green and red) (A), SRI+ (green) and SRI– (red) strains (B), two LRI– strains (green and red) (C), and LRI+ (green) and LRI– (red) strains (D). Scale bars, 2 mm. (**E**) Representative ecosystem colony images of the four microbial consortia upon reporter swapping. Top left: SRI– (red) and SRI– (green); top right: SRI+ (red) and SRI– (green); bottom left: LRI– (red) and LRI– (green); and bottom right: LRI+ (red) and LRI– (green). Scale bars, 2 mm. (**F**) Relative abundance of the green strains at the expanding fronts as a function of time.

which is primarily due to the stochasticity of the genetic drift at the expanding frontiers (*23*).

To quantify the range expansion dynamics, we analyzed the time evolution of the relative green species abundance at the expanding fronts in Fig. 2 (A to D) using a custom-tailored image processing procedure (fig. S3 and Supplementary Text). Consistent with our previous observations, the quantitative results (Fig. 2F) showed that competition favors toxin producers and that the extinction time of the sensitive species is anticorrelated to the spatial interaction scale, i.e., a longer spatial scale of interference implies a shorter extinction time of the sensitive.

To ascertain that the observations are not limited to a specific experimental setting, we systematically varied the initial conditions of the range expansion experiments (Materials and Methods). We found that, although altering the initial strain ratio changed the relative abundance at a given time (Fig. 3A, colonies in a single row), it did not change the facts that toxin producers outcompete sensitive species and that the extinction time of the sensitive under LRI is shorter than that under SRI (Fig. 3A, colonies in a single column). The findings were also quantitatively illustrated by the colony statistics in Fig. 3 (B to E): The green species abundance was determined by their initial ratios in the control consortia (Fig. 3, B and D); however, it always increased gradually over time in the SRI consortium (Fig. 3C) and remained full in the LRI consortium (Fig. 3E). We also found that our findings continued to be valid upon the variation of the initial total cell density (Fig. 3F, colonies in a single column), despite the extended survival of the sensitive species at reduced initial densities (colonies in a single row). The statistics of the colony structures from repeated experiments also supported the findings (Fig. 3, G to J). Similarly, we also examined the impact of initial cell volume on the colony development (fig. S4). Together, we concluded that, in the regimes explored, there is a reciprocal relationship of range expansion that a longer spatial scale of interference implies a shorter time for the sensitive species to extinguish at expanding fronts.

## Theory and simulation explain the space-to-time translation

To quantitatively understand the role of spatial inference scale and also to bridge the gap of the scales tested in the above experiments, we developed an individual-based community simulation program by adopting the multiscale, spatial community modeling framework that we recently developed (*39*). The program mimics the range expansion of competing communities with continuously varied interaction scales (Supplementary Text). Our simulation results (Fig. 4A) and corresponding analysis (Fig. 4B) show that, for a one-way interfering consortium (i.e., an ecosystem consisting of a toxin-producing strain and a sensitive strain) that started from a fixed initial distribution (fig. S5A), the extinction time of the sensitive species declines monotonically with the increase of the toxin diffusion constant of the producer. To confirm that our findings are not due to the evenly sectored initial condition, we repeated the individual-based simulations using a random initial condition where cells were sparsely seeded in a random fashion (fig. S6).

To gain deeper insights into the origin of the space-to-time translation, we derived a mathematical model by treating individual toxin-producing cells as point sources that emit toxins in space (Supplementary Text). Briefly, the general time evolution of toxin $T(x, t)$ can be described as $\frac{\partial T(x,t)}{\partial t} = \alpha\rho - \gamma T(x,t) + D\nabla^2 T(x,t)$, where $t$ is time, $x$ is the spatial location, $\alpha$ is the toxin production rate per cell, $\rho$ is the density of toxin producers, $\gamma$ is the toxin degradation rate, and $D$ is the diffusion constant. For a single toxin point source, the steady-state spatial distribution of toxin can be expressed as $T = \frac{\alpha}{2\gamma\xi} e^{-|x|/\xi}$, where $|x|$ refers to the distance from the source and the scale constant $\xi$ is defined as $\xi = \left(\frac{D}{\gamma}\right)^{1/2}$. This result shows that, when the distance is small compared to the diffusion scale, the interaction range of a single point source, defined as the range where the toxin concentration is over a specific threshold, is positively correlated with the toxin's diffusion constant (Fig. 4C).

During range expansion, the toxin-producing and sensitive strains form sectors in space (Fig. 2); thus, in the vicinity of each sector boundary where interference occurs, the spatial population structure can be modeled as an array of evenly distributed cells that are well segregated into toxin-producing and sensitive subpopulations (Fig. 4D). Notably, the overall toxin in space is the superposition of the toxin fields generated by individual producers (Fig. 4D), from which the averaged toxin level over all sensitive cells, $\langle T\rangle$, can be derived as $\langle T\rangle = \left(\frac{2\alpha\rho_0\xi}{\gamma L(1-f)}\right)\left(e^{-\frac{L}{2\xi}}\sinh\left(\frac{Lf}{2\xi}\right)\sinh\left(\frac{L(1-f)}{2\xi}\right)\right)$, where $\rho_0$ is the averaged cell density over space, $L$ is the dimension of the cell array, and $f$ is the fraction of the producers in the total population. Combining the above expression with the population dynamics of the two-strain ecosystem (eq. S19) leads to the extinction time of the sensitive species as

$$t_{\text{ext}} = \left(\frac{g_0 c\alpha\rho_0}{\gamma}\right)^{-1} \frac{e^{\frac{1}{z}}}{z}\int_{0.5}^{0.99} \frac{1}{f}\,\text{csch}\left(\frac{f}{z}\right)\text{csch}\left(\frac{1-f}{z}\right)df$$

where $g_0$ is the growth rate of the strains, $c$ is the sensitivity to toxin, and $z$ is a dimensionless parameter ($z = 2\xi/L$). In the regime that our

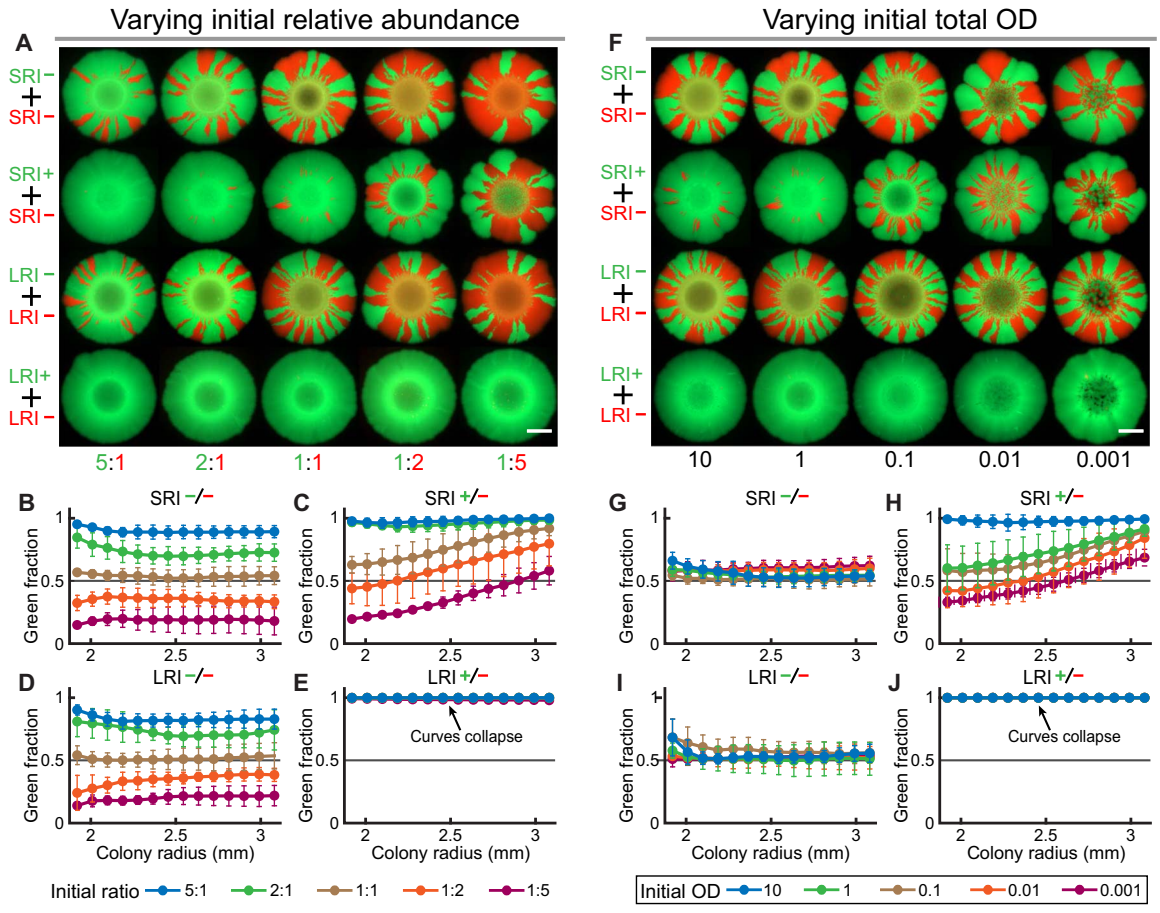


**Fig. 3. Ecosystem range expansion under different initial conditions.** (**A** and **F**) Representative fluorescence images of the consortia with altered initial ratio (A) and initial total density (F). Compared are four types of two-strain consortia, which consist of green SRI– and red SRI–, green SRI+ and red SRI–, green LRI– and red LRI–, and green LRI+ and red LRI–, accordingly. Images were taken at 80 hours after the placement of consortia droplets on agar plates. Scale bars, 2 mm. OD, optical density. (**B** to **E** and **G** to **J**) Statistics of the relative green strain abundance at the expanding fronts upon the variations of initial ratio (B to E) and initial total density (G to J). Circles and bars correspond to means and variances, respectively. Sample size, $n = 5$.

experiments explored, the extinction time indeed decays with the increase of the toxin's diffusion constant (Fig. 4E). Notably, like other theories, our findings have valid regimes; a general discussion on the extinction time–toxin diffusion relationship is provided in Supplementary Text and fig. S5B.

## Divergent spatial structures emerge from ecosystems with bidirectional interference

Other than just being unidirectional, social interactions of native microbial communities are often mutual, which motivated us to investigate the role of the spatial scale during the assemblages of microbes with bidirectional interactions. We hence constructed a consortium of two strains, namely, bSRI+ and bLRI+, which oppose each other via SRI and LRI, accordingly (Fig. 5A). Derived from the same parent strain (*E. coli* EPI300), bSRI+ and bLRI+ carry different synthetic circuits (fig. S7). The former contains the constitutively expressed contact-dependent inhibition operon *cdiBAI* and the Lux transcriptional factor *luxR* gene, as well as the AHL-inducible toxin *ccdB* gene (fig. S1E). The latter harbors the constitutively expressed *luxI* gene (fig. S1C). In addition, different fluorescence genes, *yemGFP* and *mKate2*, were integrated into their chromosomes for visualization.

To explore possible community structures of the consortium, we extended our theoretical model of toxin superposition from one-way to two-way interferences (Supplementary Text). Our calculations predicted that, depending on its initial conditions, the two-way consortium may produce opposite community structures—monotonic bSRI+ dominance or bLRI+ dominance—with the separatrix of the outcomes determined by the spatial scales of the interferences (Fig. 5B and fig. S8).

To confirm the predictions, we conducted a series of range expansion experiments for the consortium by systematically varying its initial conditions (Materials and Methods). We observed monotonic bSRI+ dominance at a high initial total density and a high initial bSRI+-to-bLRI+ ratio and bLRI+ dominance at a low total density and a low bSRI+-to-bLRI+ ratio (Fig. 5C). These structures were qualitatively different from those of the communities without interference (fig. S9) or with one-way interference (figs. S10 and S11). These structures were also not caused by the metabolic loads associated with the fluorescence reporters (Fig. 5D). Instead, the reason for the structural divergence is that, at a high initial total density, cells were tightly packed since the beginning of the experiment. Thus, bSRI+ was able to effectively inject toxins to bLRI+, while bLRI+ wasted its toxins because of long-scale diffusion, which resulted in the outperformance of bSRI+ during range

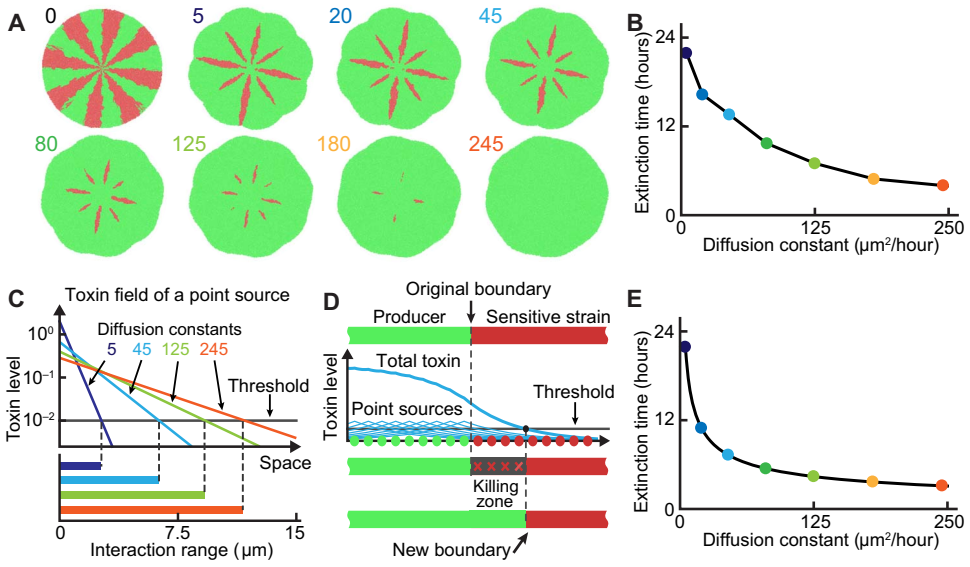


**Fig. 4. Computational simulations and theoretical analysis of the space-to-time translation during ecosystem range expansion.** (**A**) Individual-based simulations of a two-strain consortium involving one-way inhibition from the green to the red strain through toxin diffusion. Range expansions started from an identical initial condition where the two species were evenly sectored (fig. S5A). The diffusion constant was varied through the simulations. (**B**) Extinction time of the sensitive strain as a function of the diffusion constant from the simulations in (A). (**C**) Theoretical calculation of the interaction range of a single toxin-producing cell with respect to the diffusion constant. (**D**) Schematic for the superposition of individual toxin fields. The overall toxin field specifies the size of the killing zone at a producer-sensitive boundary and, hence, determines the rate of extinction of the sensitive strain. (**E**) Extinction time of the sensitive strain from the theoretical model.

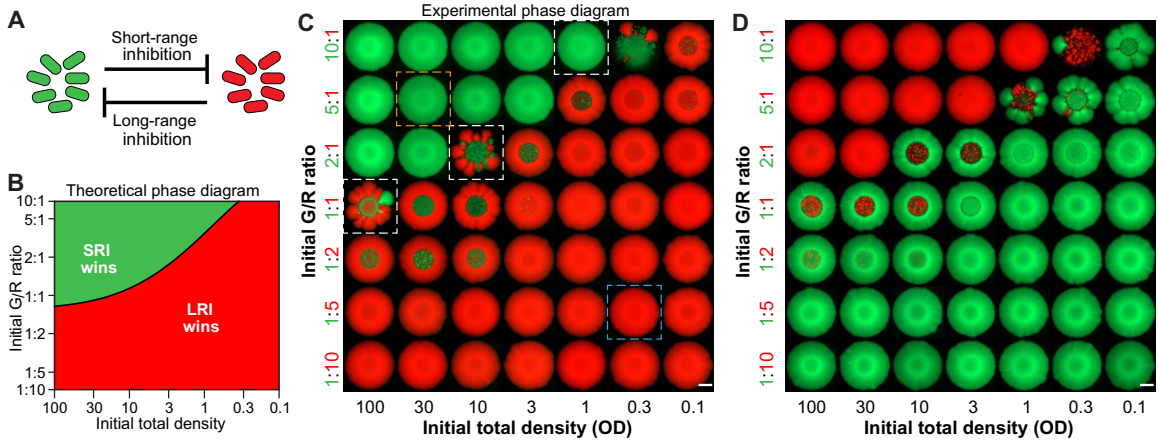


**Fig. 5. Divergent community structures formed by a consortium with bidirectional, two-scale interference.** (**A**) Schematic diagram of the consortium. The green strain (bSRI+) suppresses the red strain (bLRI+) through a contact-dependent SRI; in contrast, the red (bLRI+) opposes the green (bSRI+) via a diffusion-based LRI. A detailed circuit diagram is illustrated in fig. S7. (**B**) Theoretical prediction on possible structures of the consortium. G/R, green/red. (**C**) Representative community structures observed in the experiments. Initial ratio and total density were varied. Scale bar, 2 mm. (**D**) Representative community structures of the bidirectional interference ecosystem upon color swapping. Here, the ecosystem consists of the red bSRI+ and the green bLRI+ strains. Scale bar, 2 mm.

expansion. Conversely, at a low initial density, the average distance among cells was much larger than the spatial scale of SRI. Therefore, bSRI+ failed to deliver toxins to bLRI+ but was inhibited by the latter through diffusible AHL, leading to the dominance of bLRI+ in this scenario. In addition, the initial bSRI+-to-bLRI+ ratio contributed to the colony structure, which was simply due to the outnumbering of one strain over the other during competition.

## Noise dictates range development at the phase boundary

In addition to monotonic structures, we observed mixed, poorly developed colonies at the boundary of the two phases (Fig. 5C, white dashed boxes), which were attributed to the close contests of the two strains under these conditions. Furthermore, as ecosystem dynamics is intrinsically stochastic, we speculated that the consortium may generate variable patterns from a single initial condition, particularly when the condition is close to the phase boundary. Consistent with the speculation, the consortium deterministically yielded monotonic bSRI+ (Fig. 6A) or bLRI+ dominance (Fig. 6B) when its initial conditions were well away from the phase boundary; however, when starting at the vicinity of the boundary, the consortium developed stochastically into diverse patterns during repeated experiments (Fig. 6C).

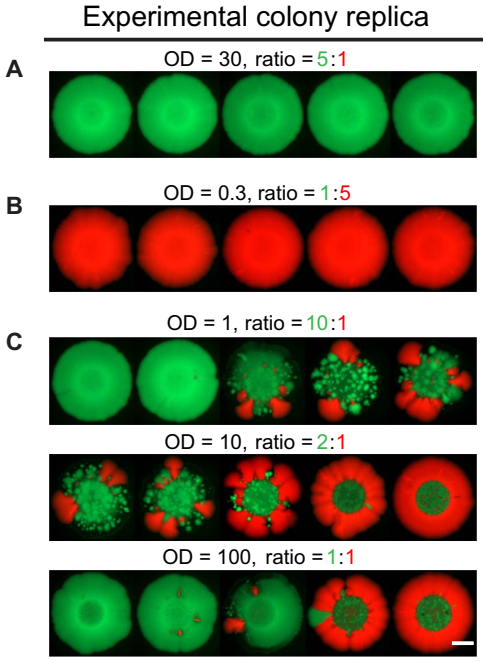


**Fig. 6. Deterministic or stochastic emergence of ecosystem structures across the phase space.** (**A**) Colony structures from repeated experiments at the initial condition of OD = 30 and 5:1 ratio, corresponding to the yellow dashed box in Fig. 5C. (**B**) Colony structures from repeated experiments at the initial condition of OD = 0.3 and 1:5 ratio, corresponding to the blue dashed box in Fig. 5C. (**C**) Colony structures from repeated experiments at the initial conditions of OD = 1.0 and 10:1 ratio, OD = 10 and 2:1 ratio, and OD = 100 and 1:1 ratio, corresponding to the three white dashed boxes in Fig. 5C. Scale bar, 2 mm.

## DISCUSSION

Our results demonstrate that the spatial scale of interaction is a critical parameter that determines the range expansion of microbial ecosystems in space. Although natural communities are considerably more complex than our engineered systems, the lessons learned from this work may provide general insights into the fundamentals of microbial ecosystem development. For example, the space-to-time translation under one-way interference exemplifies the theory that unifies the spatial and temporal characteristics of ecosystems through scales (*9*, *40*). In addition, the emergence of diverse community structures in a two-way interference upon the variation of initial conditions may offer an alternative mechanism for the maintenance of biological diversity. This knowledge will advance our basic understanding about spatial microbial ecology, helping to elucidate the structures of native communities such as those in the human gut and in the rhizosphere (*41*).

Notably, in addition to the spatial scale of social interactions, there are multiple other factors such as nutrient availability and agar surface friction that contribute to microbial range expansion. For example, in a setting with a reduced nutrient availability, growing bacteria can develop into branched, finger-like structures that physically separate cells into clusters (*2*). As a result, the average distance between cells increases, consequently reducing the strengths of both the short- and long-range interactions in modulating colony structures. However, we expect that such a morphological change has a more substantial impact on the short-range case because more sensitive cells will be out of the interaction range due to branch formation. Similarly, increasing the surface friction will promote cell aggregation and, hence, average cellular distances, resulting in the augment of the numbers of interfering cells and the strength of cellular interference. In this circumstance, we speculate that both the short- and long-range interactions will be increased but that the former has a more substantial augment due to its local nature.

Although this study has focused on microbial populations, spatial scale variation of cellular interactions is commonly observed in multicellular organisms as well. For instance, in animals and plants, juxtacrine signaling involves direct contact between signal molecules in the membrane of the signal-transmitting cells and receptor proteins in the membrane of target cells [e.g., notch signaling (*42*)], paracrine signaling enables local interactions through the secretion and detection of locally diffusible molecules [e.g., neurotransmitters (*43*)], while endocrine signaling confers distant interactions throughout a whole organism via long-range diffusive molecules [e.g., hormones (*44*)]. We thus speculate that the roles of the spatial interaction scale revealed in microbial range expansion may be translatable to cellular signaling in multicellular organisms, thus shedding light on the organizational rules underlying multicellularity of higher organisms.

Last, engineered microbial consortia have recently emerged as a promising frontier of synthetic biology because of their expanded functional programmability and increased circuit robustness compared to those of synthetic single populations (*20*). On that front, understanding spatial scale is highly valuable for design, construction, and optimization of artificial microbial ecosystems with desired spatial and temporal structures, thereby benefiting the creation of ecosystem-based gene circuits for next-generation biotechnological applications.

## MATERIALS AND METHODS

### Bacteria and growth conditions

Strains used in this study are all listed in table S1. *E. coli* 10-beta (New England BioLabs) was used in all cloning steps. *E. coli* EPI300 (Epicentre) and its derivatives were used to perform both single-cell and droplet competition experiments throughout the study. All *E. coli* strains were grown in LB medium at 37°C, unless indicated otherwise. If needed, then antibiotics were added using the following final concentrations: chloramphenicol (Cm; 25 μg $ml^{-1}$) and kanamycin (Kan; 50 μg $ml^{-1}$).

### Plasmid and strain construction

The plasmid with the SRI+ phenotype (pCC-CDI) was constructed from the plasmid pDAL661 (*45*) by introducing a constitutive promoter J23119 (http://parts.igem.org/Main_Page) upstream of the contact-dependent inhibition (CDI) operon. The copy-controlled plasmid, pCC1BAC, was purchased from Epicentre and used in the SRI– phenotype. The plasmid with the LRI+ phenotype (pCC-AHL) was constructed by cloning a constitutive $P_{trc}$ promoter from pChemoK (*46*), the *luxI* gene, and the rnpT1 terminator into the pCC1BAC vector. The plasmid with LRI– phenotype (pCC-CcdB) has a copy of the AHL-inducible *ccdB* gene. It was constructed by cloning the luxR-$P_{luxR}$-$P_{luxI}$ cassette from pTD103LuxI_sfGFP (*47*), a mutant version of *ccdB* gene (*ccdB* [9delA], a truncated *ccdB* gene with a reduced toxicity) and rnpT1 into pCC1BAC. The plasmid pCC-CDI-CcdB was constructed from pCC-CDI by introducing the AHL-inducible *ccdB* gene from pCC-CcdB. It was used in conjugation with the plasmid pCC-AHL for bidirectional competition.

All plasmid components were used as untagged except for *luxI*, which has a 3′ ssrA degradation tag (AANDENYALAA) for rapid protein degradation (*48*). All plasmids used in this study have the same

backbone as the plasmid pCC1BAC. The copy number of the plasmids can be switched from single to multiple (~10 to 12) upon induction with either CopyControl Induction Solution provided by the manufacturer or L-(+)-arabinose solution [0.2% (w/v)]. The plasmid maps and their characteristics are listed in fig. S1. GenBank accession numbers for SRI and LRI plasmids are as follows: MG867730, MG867731, MG867732, and MG867733.

Two *E. coli* EPI300 strains that constitutively express yemGFP or mKate2 (EPI300 lacZ::$P_{J23119}$-yemGFP and EPI300 lacZ::$P_{J23119}$-mKate2) were constructed with a lambda Red–mediated homologous recombination system by replacing lacZ with $P_{J23119}$-driven *yemGFP* or *mKate2* using modified pKD4 plasmids, pKD4-$P_{J23119}$-yemGFP and pKD4-$P_{J23119}$-mKate2, as previously described (*49*). The resulting strains, used in range expansion experiments, were named as EPI300-yemGFP and EPI300-mKate2. Another two strains (EPI300-P21-yemGFP and EPI300-P21-mKate2) that have stronger fluorescence expression were constructed for single-cell experiments using the clonetegration method through the integration of $P_{J23119}$-yemGFP or $P_{J23119}$-mKate2 into the attB site of phage P21 on the chromosome of EPI300 (*50*). All strains used in this study are described in table S1.

### Single-cell fluorescence microscopy

Single-cell time-lapse fluorescence microscopy experiments were performed as described previously with modifications (*51*, *52*). An M9 minimal medium was prepared as follows: 1.5% (w/v) agarose was dissolved in M9 minimal medium (1× M9 salts, 0.4% glucose, 2 mM MgSO4, 0.1 mM CaCl2, 0.00005% thiamine hydrochloride, and 0.1% casamino acids) with slow heating in a microwave. After adding Cm and arabinose [0.2% (w/v)], the molten medium was poured onto a glass slide, and then, a cover slide was put on the top immediately. After solidification for 1 hour at 4°C, 1 to 2 μl of diluted exponentially growing cultures were pipetted onto an agarose pad. After drying for 10 to 15 min at room temperature, the agarose pad was flipped onto a glass-bottom dish with a lid to prevent edge evaporation. Image acquisition was then performed on an AMG EVOS FL microscope. Images were acquired by phase-contrast microscopy and in green/red fluorescence channels every 30 min.

### CcdB induction experiment

The toxicity of the mutant *ccdB* gene, *ccdB* [9delA], was tested through its growth inhibition activity. EPI300-mKate2/pCC-CcdB and EPI300-mkate2/pCC1BAC (*ccdB*$^-$ controls) were cultured overnight and subinoculated to fresh LB/Cm/arabinose at a 1:100 dilution. When the $OD_{600}$ (optical density at 600 nm) of the culture reached 0.4, *N*-(3-oxohexanoyl)-L-homoserine lactone (Chemodex) was added to the culture at the final concentrations of 0.1 and 10 μM for induction. The $OD_{600}$ of the cultures was measured every hour until the culture reached the stationary phase.

### Competition assays in liquid culture

Single-strain cultures of SRI+, SRI−, SRI+(kan), SRI−(kan), LRI+, LRI−, LRI+(kan), and LRI−(kan) were grown overnight (16 hours) in LB/Cm/arabinose medium and then subinoculated into fresh media at 1:100 dilution and grown to an $OD_{600}$ of 0.35. Equal volume of two cultures were mixed in the following combinations: SRI+/SRI−(kan), SRI+/SRI+(kan), SRI−/SRI−(kan), LRI+/LRI−(kan), LRI+/LRI+(kan), and LRI−/LRI−(kan). The well-mixed cultures were further grown at 37°C with shaking at 225 rpm for another 4 hours. Samples were taken from the mixed culture hourly, and colony-forming units of Kan-resistant cells were determined through serial dilution and plate counting with Kan selection.

### Range expansion experiments of one-way competing consortia on solid agar

SRI+, SRI−, LRI+, and LRI− strains were separately grown overnight (16 hours) in LB/Cm medium to stationary phase. Then, cells were subinoculated to 5 ml of LB/Cm medium supplemented with 1× CopyControl Induction Solution in a 50-ml Falcon tube at 1:10 dilution and incubated at 37°C with shaking at 225 rpm for 5 hours. Toxin-producing and sensitive cells were adjusted to an $OD_{600}$ of 1.0 using fresh medium and mixed at 1:1 ratio for different combinations. Aliquots (1 μl) of each combination were spotted onto LB/Cm agar (15 ml of 1.5% agar in a 90-mm plate) containing arabinose [0.2% (w/v)] and incubated at 37°C. Green and red fluorescence of the colonies were imaged using a Zeiss Axio Zoom.V16 microscope with an AxioCam HRm camera at 12, 24, 36, 48, 72, and 96 hours. In addition, toxin-producing and sensitive cells were mixed at total $OD_{600}$ = 1 but with different initial ratios (5:1 to 1:5) and with 1:1 ratio but at different initial total $OD_{600}$. The cell mixtures were spotted onto an agar plate as above and incubated at 37°C for imaging at 80 hours.

### Range expansion experiments of bidirectional competing consortia on solid agar

Single strains of bSRI+ and bLRI+ were grown in LB/Cm/arabinose medium with shaking at 225 rpm and 37°C for 16 hours. Then, the cultures were inoculated at 1:10 dilution into fresh LB/Cm/arabinose medium at 37°C for 5 hours. The $OD_{600}$ of the two competitor cultures was adjusted to different levels, from 100 to 0.1, using centrifugation or dilution with fresh LB/Cm/arabinose medium. The two cultures were then mixed at different ratios from 10:1 to 1:10. One microliter of aliquot was immediately dropped onto an agar plate (15 ml of LB/Cm/arabinose with 1.5% agar in a 90-mm plate). Droplets were allowed to dry at room temperature for 1 hour, and then, the plates were incubated at 37°C for 80 hours. Control experiments that use the combinations of LRI−/LRI−, bSRI+/LRI−, and LRI−/LRI+ were also investigated. Images were acquired by using a Zeiss Axio Zoom. V16 microscope with an AxioCam HRm camera.

### Image processing

To quantify colony statistics, Mathematica was used to extract data from the colony images. The following procedure was used (fig. S3): First, background pixels were set to black. Second, the center of mass for the colored pixels was located along with the edge of the colony. Third, each remaining colored pixel was converted in a binary fashion to green or red, depending on the dominant RGB (red, green, blue) value. Connected clusters of red and green pixels were determined for radial cross sections of the colony. Fourth, numbers of red and green pixels in a given cross section were used to determine the statistics of the abundance of each species.

### Individual-based simulations and mathematical modeling

Individual-based simulations of community range expansion were developed by explicitly considering cellular movement, nutrient utilization, growth, and toxin-mediated inhibitions in space. Notably, cellular movement caused by cellular mechanical forces was modeled in the same ways as our previous work (*39*); the remaining processes are

detailed in Supplementary Text. Mathematical models were also constructed using partial differential equations to provide biophysical insights into spatial interaction scale. By considering a single producer cell as a point source of toxin, communities of microbes were described as the superposition of point sources that were distributed in space. Analysis of the models allowed driving the extinction time of the sensitive species in one-way competition and the phase boundary of two-way competition. Details of the mathematical models are provided in Supplementary Text.

## SUPPLEMENTARY MATERIALS

Supplementary material for this article is available at http://advances.sciencemag.org/cgi/content/full/4/11/eaau0695/DC1

Supplementary Text

Fig. S1. Plasmids used in this study.

Fig. S2. Characterizations of the strain carrying the mutant *CcdB* gene and competition assays of SRI and LRI in liquid cultures.

Fig. S3. Schematic of imaging processing.

Fig. S4. Representative fluorescence images of the consortia with altered initial culture volume.

Fig. S5. Simulation initial conditions and theoretical extinction time.

Fig. S6. Individual-based simulations of colony expansion from a randomly sampled initial population.

Fig. S7. Circuit design of bidirectional competition.

Fig. S8. Alteration of the phase diagram of the bidirectionally competing consortium by the relative spatial scales of interference.

Fig. S9. Representative images of the consortium consisting of EPI300-yemGFP/pCC-CcdB and EPI300-mKate2/pCC-CcdB.

Fig. S10. Representative images of the consortium composed of EPI300-yemGFP/pCDI-CcdB and EPI300-mKate2/pCC-CcdB.

Fig. S11. Representative images of the consortium consisting of EPI300-yemGFP/pCC-CcdB and EPI300-mKate2/pCC-AHL.

Table S1. Strains used in this study.

References (*53*)

## REFERENCES AND NOTES


1. M. Matsushita, J. Wakita, H. Itoh, I. Ràfols, T. Matsuyama, H. Sakaguchi, M. Mimura, Interface growth and pattern formation in bacterial colonies. *Physica A* **249**, 517–524 (1998).
2. E. Ben-Jacob, I. Cohen, H. Levine, Cooperative self-organization of microorganisms. *Adv. Phys.* **49**, 395–554 (2000).
3. E. O. Budrene, H. C. Berg, Complex patterns formed by motile cells of *Escherichia coli*. *Nature* **349**, 630–633 (1991).
4. P. Stoodley, K. Sauer, D. Davies, J. W. Costerton, Biofilms as complex differentiated communities. *Annu. Rev. Microbiol.* **56**, 187–209 (2002).
5. J. W. Costerton, P. S. Stewart, E. P. Greenberg, Bacterial biofilms: A common cause of persistent infections. *Science* **284**, 1318–1322 (1999).
6. R. M. Atlas, R. Bartha, *Microbial Ecology: Fundamentals and Applications* (Addison-Wesley Pub. Co., 1981).
7. K. Faust, J. Raes, Microbial interactions: From networks to models. *Nat. Rev. Microbiol.* **10**, 538–550 (2012).
8. J. B. Xavier, Social interaction in synthetic and natural microbial communities. *Mol. Syst. Biol.* **7**, 483 (2011).
9. D. Tilman, P. M. Kareiva, *Spatial Ecology: The Role of Space in Population Dynamics and Interspecific Interactions* (Princeton Univ. Press, 1997).
10. L. McNally, E. Bernardy, J. Thomas, A. Kalziqi, J. Pentz, S. P. Brown, B. K. Hammer, P. J. Yunker, W. C. Ratcliff, Killing by type VI secretion drives genetic phase separation and correlates with increased cooperation. *Nat. Commun.* **8**, 14371 (2017).
11. B. L. Bassler, R. Losick, Bacterially speaking. *Cell* **125**, 237–246 (2006).
12. S. K. Kim, D. Kaiser, C-factor: A cell-cell signaling protein required for fruiting body morphogenesis of *M. xanthus*. *Cell* **61**, 19–26 (1990).
13. R. Losick, P. Stragier, Crisscross regulation of cell-type-specific gene expression during development in *B. subtilis*. *Nature* **355**, 601–604 (1992).
14. S. K. Aoki, R. Pamma, A. D. Hernday, J. E. Bickham, B. A. Braaten, D. A. Low, Contact-dependent inhibition of growth in *Escherichia coli*. *Science* **309**, 1245–1248 (2005).
15. A. Prindle, J. Liu, M. Asally, S. Ly, J. Garcia-Ojalvo, G. M. Süel, Ion channels enable electrical communication in bacterial communities. *Nature* **527**, 59–63 (2015).
16. A. Eberhard, A. L. Burlingame, C. Eberhard, G. L. Kenyon, K. H. Nealson, N. J. Oppenheimer, Structural identification of autoinducer of *Photobacterium fischeri* luciferase. *Biochemistry* **20**, 2444–2449 (1981).
17. L. M. Mashburn, M. Whiteley, Membrane vesicles traffic signals and facilitate group activities in a prokaryote. *Nature* **437**, 422–425 (2005).
18. S. A. Levin, The problem of pattern and scale in ecology: The Robert H. MacArthur Award lecture. *Ecology* **73**, 1943–1967 (1992).
19. M. G. Turner, R. H. Gardner, R. V. O'neill, *Landscape Ecology in Theory and Practice* (Springer, 2001).
20. K. Brenner, L. You, F. H. Arnold, Engineering microbial consortia: A new frontier in synthetic biology. *Trends Biotechnol.* **26**, 483–489 (2008).
21. K. R. Foster, T. Bell, Competition, not cooperation, dominates interactions among culturable microbial species. *Curr. Biol.* **22**, 1845–1850 (2012).
22. R. M. Donlan, Biofilms: Microbial life on surfaces. *Emerg. Infect. Dis.* **8**, 881–890 (2002).
23. O. Hallatschek, P. Hersen, S. Ramanathan, D. R. Nelson, Genetic drift at expanding frontiers promotes gene segregation. *Proc. Natl. Acad. Sci. U.S.A.* **104**, 19926–19930 (2007).
24. M. S. Datta, K. S. Korolev, I. Cvijovic, C. Dudley, J. Gore, Range expansion promotes cooperation in an experimental microbial metapopulation. *Proc. Natl. Acad. Sci. U.S.A.* **110**, 7354–7359 (2013).
25. A. Templeton, Out of Africa again and again. *Nature* **416**, 45–51 (2002).
26. R. A. Duckworth, A. V. Badyaev, Coupling of dispersal and aggression facilitates the rapid range expansion of a passerine bird. *Proc. Natl. Acad. Sci. U.S.A.* **104**, 15017–15022 (2007).
27. B. L. Phillips, G. P. Brown, J. K. Webb, R. Shine, Invasion and the evolution of speed in toads. *Nature* **439**, 803 (2006).
28. B. Kerr, M. A. Riley, M. W. Feldman, B. J. M. Bohannan, Local dispersal promotes biodiversity in a real-life game of rock–paper–scissors. *Nature* **418**, 171–174 (2002).
29. W. Weber, M. Daoud-El Baba, M. Fussenegger, Synthetic ecosystems based on airborne inter- and intrakingdom communication. *Proc. Natl. Acad. Sci. U.S.A.* **104**, 10435–10440 (2007).
30. F. K. Balagaddé, H. Song, J. Ozaki, C. H. Collins, M. Barnet, F. H. Arnold, S. R. Quake, L. You, A synthetic *Escherichia coli* predator–prey ecosystem. *Mol. Syst. Biol.* **4**, 187 (2008).
31. J. S. Chuang, O. Rivoire, S. Leibler, Simpson's paradox in a synthetic microbial system. *Science* **323**, 272–275 (2009).
32. E. H. Wintermute, P. A. Silver, Emergent cooperation in microbial metabolism. *Mol. Syst. Biol.* **6**, 407 (2010).
33. L. Dai, D. Vorselen, K. S. Korolev, J. Gore, Generic indicators for loss of resilience before a tipping point leading to population collapse. *Science* **336**, 1175–1177 (2012).
34. H. Youk, W. A. Lim, Secreting and sensing the same molecule allows cells to achieve versatile social behaviors. *Science* **343**, 1242782 (2014).
35. J. Gore, H. Youk, A. Van Oudenaarden, Snowdrift game dynamics and facultative cheating in yeast. *Nature* **459**, 253–256 (2009).
36. W. Kong, D. R. Meldgin, J. J. Collins, T. Lu, Designing microbial consortia with defined social interactions. *Nat. Chem. Biol.* **14**, 821–829 (2018).
37. C. M. Waters, B. L. Bassler, Quorum sensing: Cell-to-cell communication in bacteria. *Annu. Rev. Cell Dev. Biol.* **21**, 319–346 (2005).
38. H. Engelberg-Kulka, G. Glaser, Addiction modules and programmed cell death and antideath in bacterial cultures. *Annu. Rev. Microbiol.* **53**, 43–70 (1999).
39. A. E. Blanchard, T. Lu, Bacterial social interactions drive the emergence of differential spatial colony structures. *BMC Syst. Biol.* **9**, 59 (2015).
40. S. A. Levin, Multiple scales and the maintenance of biodiversity. *Ecosystems* **3**, 498–506 (2000).
41. C. D. Nadell, K. Drescher, K. R. Foster, Spatial structure, cooperation and competition in biofilms. *Nat. Rev. Microbiol.* **14**, 589–600 (2016).
42. S. Artavanis-Tsakonas, M. D. Rand, R. J. Lake, Notch signaling: Cell fate control and signal integration in development. *Science* **284**, 770–776 (1999).
43. H. Lodish, A. Berk, S. L. Zipursky, P. Matsudaira, D. Baltimore, J. Darnell, *Molecular Cell Biology* (W. H. Freeman, 2000).
44. N. Neave, *Hormones and Behaviour: A Psychological Approach* (Cambridge Univ. Press, 2007).
45. S. K. Aoki, E. J. Diner, C. t. K. de Roodenbeke, B. R. Burgess, S. J. Poole, B. A. Braaten, A. M. Jones, J. S. Webb, C. S. Hayes, P. A. Cotter, D. A. Low, A widespread family of polymorphic contact-dependent toxin delivery systems in bacteria. *Nature* **468**, 439–442 (2010).
46. T. S. Moon, E. J. Clarke, E. S. Groban, A. Tamsir, R. M. Clark, M. Eames, T. Kortemme, C. A. Voigt, Construction of a genetic multiplexer to toggle between chemosensory pathways in *Escherichia coli*. *J. Mol. Biol.* **406**, 215–227 (2011).
47. A. Prindle, P. Samayoa, I. Razinkov, T. Danino, L. S. Tsimring, J. Hasty, A sensing array of radically coupled genetic 'biopixels'. *Nature* **481**, 39–44 (2012).
48. J. B. Andersen, C. Sternberg, L. K. Poulsen, S. P. Bjørn, M. Givskov, S. Molin, New unstable variants of green fluorescent protein for studies of transient gene expression in bacteria. *Appl. Environ. Microbiol.* **64**, 2240–2246 (1998).

49. K. A. Datsenko, B. L. Wanner, One-step inactivation of chromosomal genes in *Escherichia coli* K-12 using PCR products. *Proc. Natl. Acad. Sci. U.S.A.* **97**, 6640–6645 (2000).
50. F. o. St-Pierre, L. Cui, D. G. Priest, D. Endy, I. B. Dodd, K. E. Shearwin, One-step cloning and chromosomal integration of DNA. *ACS Synth. Biol.* **2**, 537–541 (2013).
51. J. W. Young, J. C. W. Locke, A. Altinok, N. Rosenfeld, T. Bacarian, P. S. Swain, E. Mjolsness, M. B. Elowitz, Measuring single-cell gene expression dynamics in bacteria using fluorescence time-lapse microscopy. *Nat. Protoc.* **7**, 80–88 (2012).
52. S. O. Skinner, L. A. Sepúlveda, H. Xu, I. Golding, Measuring mRNA copy number in individual *Escherichia coli* cells using single-molecule fluorescent in situ hybridization. *Nat. Protoc.* **8**, 1100–1113 (2013).
53. J. H. Espenson, *Chemical Kinetics and Reaction Mechanisms* (McGraw-Hill, 1995).

**Acknowledgments:** We thank D. Low and C. Voigt for gifts of DNA materials. **Funding:** This work was supported by the NSF (1553649 and 1227034), the Office of Naval Research (N000141612525), the American Heart Association (12SDG12090025), the Brain and Behavior Research Foundation, and the National Center for Supercomputing Applications. V.C.O. was supported by the Council of Higher Education (YOK) of Turkey. **Author contributions:** T.L. conceived the project, designed the study, and supervised the project. V.C.O. and W.K. performed the experiments. V.C.O., W.K., A.E.B., F.L., and T.L. analyzed the experimental data. A.E.B. performed the computational modeling. A.E.B and T.L. analyzed the simulations. T.L., W.K., and A.E.B. wrote the manuscript. **Competing interests:** The authors declare that they have no competing interests. **Data and materials availability:** All data needed to evaluate the conclusions in the paper are present in the paper and/or the Supplementary Materials. Additional data related to this paper may be requested from the authors.

Submitted 12 May 2018
Accepted 23 October 2018
Published 21 November 2018
10.1126/sciadv.aau0695

**Citation:** V. Celik Ozgen, W. Kong, A. E. Blanchard, F. Liu, T. Lu, Spatial interference scale as a determinant of microbial range expansion. *Sci. Adv.* **4**, eaau0695 (2018).